Artigo recebido em 22/01/2026
Aceito em 04/05/2026
Revista SODEBRAS – Volume 20 N° 224

IMPACT OF DC-ARRAY FAULTS, PARTIAL SHADING, AND SINGLE-PHASE-TO-GROUND FAULTS ON PHOTOVOLTAIC SYSTEMS

Lucas Moraes Rego Cruz[1]
Fernando Augusto Moreira[2]
Felipe Mendes De Vasconcellos[3]

Resumo – Este artigo investiga a resposta dinâmica de um sistema fotovoltaico (FV) de 50,7 kW conectado à rede elétrica sob diferentes cenários de contingência. Foi desenvolvido um modelo detalhado em Matlab/Simulink, composto por um arranjo fotovoltaico de 238 módulos, um conversor CC–CC do tipo boost controlado por um algoritmo de MPPT Perturba e Observa (P&O) e um inversor trifásico CC–CA conectado a uma rede elétrica de 120 V e 60 Hz. O estudo avalia o comportamento do sistema durante distúrbios internos no lado CC (circuito aberto, curto-circuito e sombreamento parcial de 1000 W/m² para 500 W/m²) e durante uma falta externa fase-terra no lado CA. A principal contribuição técnica consiste em quantificar o impacto dessas faltas sobre a estabilidade da tensão nominal de 800 V do barramento CC, sobre o fluxo de potência ativa e sobre a qualidade das correntes CA. Os resultados demonstram que, embora o sistema se recupere de forma eficaz após faltas no lado CC, as faltas no lado da rede impõem severos esforços elétricos, como sobretensões no barramento CC de até 4000 V. Isso evidencia a necessidade crítica de capacidade coordenada de ride-through e de estratégias de proteção contra sobretensões em sistemas fotovoltaicos conectados à rede.

Palavras-chave: Energia solar. Sistemas fotovoltaicos. Integração à rede elétrica. Modelagem e simulação. Rastreamento do ponto de máxima potência (MPPT).

Abstract – This paper investigates the dynamic response of a 50.7 kW grid-connected photovoltaic (PV) system under various contingency scenarios. A detailed Matlab/Simulink model was developed, comprising a 238-module PV array, a boost DC–DC converter controlled by a Perturb and Observe (P&O) MPPT algorithm, and a three-phase DC–AC inverter connected to a 120 V, 60 Hz electrical grid. The study evaluates the system's behavior during internal DC-side disturbances (open-circuit, short-circuit, and partial shading from 1000 W/m² to 500 W/m²) and an external AC-side single-phase-to-ground fault. The main technical contribution lies in quantifying the impact of these faults on the nominal 800 V DC-link voltage stability, active power flow, and AC current quality. The results demonstrate that while the system can effectively recover after fault conditions on the DC side, grid-side faults impose severe electrical stress, such as DC-link overvoltage up to 4000 V. This highlights the critical need for coordinated ride-through capabilities and overvoltage protection strategies in grid-connected PV systems.

Keywords: Solar energy. Photovoltaic systems. Grid integration. Modelling and simulation. Maximum power point tracking (MPPT).

I. INTRODUCTION

The global transition towards renewable energy has driven a significant increase in the integration of photovoltaic (PV) systems into electrical grids. In countries like China and Germany, effective public policies have established solar energy as a major, successful component of their electricity generation (YAO; CAI, 2019; GRAU; HUO; NEUHOFF, 2012). In Brazil, where the electrical energy matrix is historically dominated by hydroelectric power (ANEEL, 2024), solar energy has experienced expressive growth, largely boosted by regulatory incentives such as the ANEEL Normative Resolution No. 482 for distributed generation (ANEEL, 2012). However, this large-scale integration introduces critical operational challenges related to power quality, system stability, and protection against electromagnetic transients. Ensuring reliable operation requires robust control strategies and accurate mathematical modeling to dynamically adapt to environmental changes and grid conditions.

During their lifespan, grid-connected PV systems are exposed to various disturbances that can compromise power extraction, which is naturally limited compared to consumer demand. On the DC side, internal faults such as

[1] MSc student in Electrical Engineering at the Federal University of Bahia (UFBA). Salvador – BA, Brazil. E-mail: lucasmoraesregocruz@gmail.com
[2] Post-Doctor in Electrical Engineering. Professor at the Department of Electrical Engineering, Federal University of Bahia (UFBA). Salvador – BA, Brazil. E-mail: moreiraf@ufba.br
[3] Post-Doctor in Electrical Engineering. Professor at the Department of Electrical Engineering, Federal University of Bahia (UFBA). Salvador – BA, Brazil. E-mail: felipe.vasconcellos@ufba.br

open-circuits, short-circuits between modules, and sudden partial shading can severely affect Maximum Power Point Tracking (MPPT) efficiency and cause power fluctuations (SUSKIS; GALKIN, 2013; ABDELSALAM et al., 2011). On the AC side, asymmetrical grid faults, such as single-phase-to-ground short-circuits, propagate voltage sags and unbalances that directly impact the inverter's performance and the stability of the DC-link.

While extensive research has focused on optimizing MPPT algorithms under normal operating or shading conditions, there is a lack of analysis regarding the electromagnetic transients and electrical stress imposed on the entire conversion chain during severe faults. Therefore, the main technical contribution of this paper is to evaluate and quantify the dynamic response and electrical tolerance limits of a grid-connected PV system under both DC-array and AC-grid faults. By analyzing variables such as DC-link voltage overshoot, recovery time, and active power flow, this study provides critical insights into the necessity of overvoltage protection and fault ride-through strategies.

This paper is organized as follows: Section II describes the methodology adopted for the modelling and simulation of the grid-connected photovoltaic system, including the photovoltaic array considered (2.1), the MPPT technique and its implementation (2.2), the sizing of the DC–DC converter (2.3) and the implementation of the different fault scenarios (2.4). Section III presents and discusses the simulation results obtained for the system under DC- and AC-side faults. Finally, Section IV presents the conclusions of the work.

II. METHODOLOGY

The modelling of the grid-connected photovoltaic system was carried out using Matlab/Simulink. To accurately capture the fast electromagnetic transients during fault conditions, the simulation was configured with a discrete fixed-step solver using a time step of 1 μs. The initial conditions were set to zero, allowing the system to naturally reach steady-state before any disturbance is applied. The developed model includes the components required for the operation of a grid-integrated solar system, such as solar panels, DC–DC converters, DC–AC inverters, and a maximum power point tracking (MPPT) algorithm.

The photovoltaic modules were modelled based on an equivalent circuit that includes a current source dependent on irradiance, a series resistance representing ohmic losses along the path of charge carriers, and a shunt resistance modelling leakage paths in the diode (CELIK; ACIKGOZ, 2007; TSAI; TU; SU, 2008). Furthermore, a DC–DC boost converter was implemented, whose duty cycle is controlled according to the MPPT algorithm to regulate the DC-link. The three-phase DC–AC inverter was chosen so as to deliver the generated energy within the standard voltage (120 V rms) and frequency (60 Hz) adopted by the electrical grid.

The system was simulated under different fault scenarios. First, an open-circuit fault and a short-circuit fault within the photovoltaic array, as well as a sudden partial shading condition, were considered. Afterwards, a single-phase-to-ground fault at the grid side was simulated. The model validation criterion was based on ensuring that, under pre-fault standard test conditions, the extracted active power and DC-link voltage closely matched the theoretical nominal values of the PV array (50.7 kW), confirming the steady-state accuracy before fault application. This methodology enabled the creation of a detailed model capable of providing a basis for the analysis and optimization of grid-connected photovoltaic systems operating under adverse scenarios.

2.1. Photovoltaic array used

The photovoltaic generator used in the fault studies consists of polycrystalline modules Soltech model 1STH-215-P. This specific module was selected as it is a standard pre-parameterized benchmark available in the Matlab/Simulink Simscape Electrical library. Its widespread adoption in recent literature ensures the reproducibility of the simulation and allows for a reliable comparison of the dynamic responses with other grid-connected PV studies (NKAMBULE; HASAN; ALI, 2019; ZAID et al., 2023).

The power at the maximum power point, under standard test conditions (i.e., 25 °C and irradiance of 1000 W/m²), is 215 W per unit. Each module has a short-circuit current of 7.84 A and an open-circuit voltage of 36.6 V. The complete array was configured with 14 modules in series per string and 17 strings in parallel, totaling 238 modules. In this topology, the open-circuit voltage per string reaches $14 \times 36.6 = 512.4$ V, while the overall short-circuit current reaches $17 \times 7.84 = 133.3$ A. Consequently, the theoretical maximum power of the photovoltaic system under standard test conditions is 50.73 kW. This value is used as a reference both for parameterizing the MPPT algorithm and for defining the pre-fault conditions analyzed in this work.

2.2. Maximum power point tracking

Maximum Power Point Tracking (MPPT) comprises techniques used in solar power systems to achieve maximum efficiency in electrical power generation, even under variations of parameters such as irradiance and temperature (ALDWANE, 2014; KADEVAL; PATEL, 2021). Due to the non-linear power–voltage characteristic of a photovoltaic module, the basic premise of MPPT algorithms is to dynamically adjust the operating voltage to track the maximum power point (FARANDA; LEVA, 2008). The execution logic of the algorithm adopted in this work is detailed in Figure 1.

Figure 1 – Example of MPPT operation.

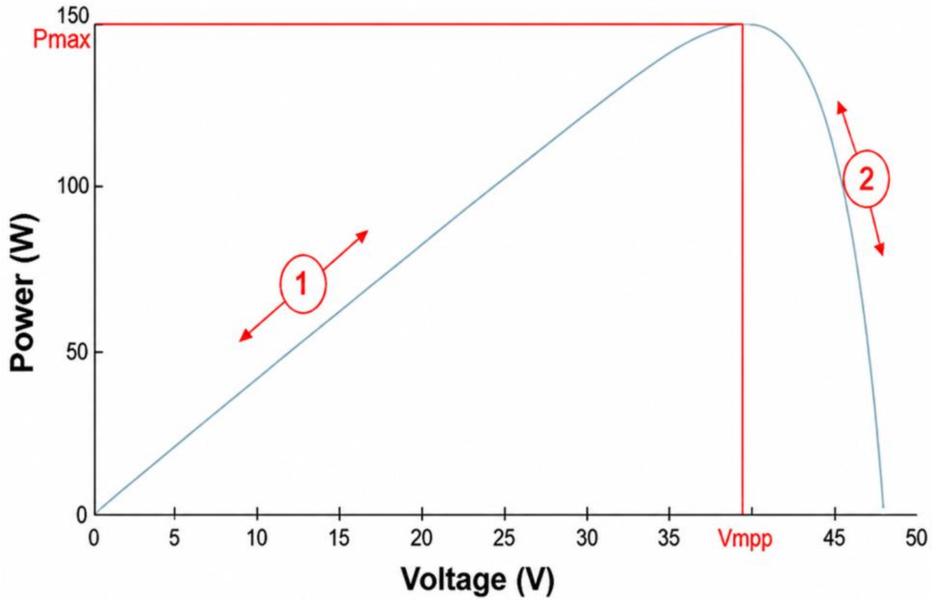

Source: The authors, 2026.

2.2.1. Perturb and observe

In this work, the Perturb and Observe (P&O) method was implemented to control the energy extraction. The MPPT controller periodically monitors the output power of the solar array by measuring voltage and current. Based on these measurements, the algorithm computes the current power, compares it with the previous iteration, and incrementally adjusts the duty cycle of the DC–DC boost converter (KRISHNARAM et al., 2024).

In the developed model, the P&O algorithm was implemented using a Simulink S-function block that directly commands the switching gate of the boost converter. While the P&O method is widely adopted for its simplicity, it is known to produce steady-state oscillations around the maximum power point and can momentarily track local maxima under rapidly changing partial shading conditions (GIRGIS; ELKHATEEB, 2024). In this study, the dynamic response of the MPPT is a critical factor, as its ability to quickly converge after severe DC-side and AC-side faults directly impacts the DC-link voltage stability and the overall energy recovery of the system.

2.3. Converter design

The DC–DC boost converter, whose topology is illustrated in Figure 2, is responsible for stepping up the output voltage of the photovoltaic array to meet the DC-link requirements of the grid-tied inverter. Furthermore, it acts as the physical actuator for the MPPT algorithm, which dynamically adjusts the converter’s duty cycle (D) to maximize energy extraction under varying solar conditions.

Figure 2 – DC–DC (boost) converter used in the system.

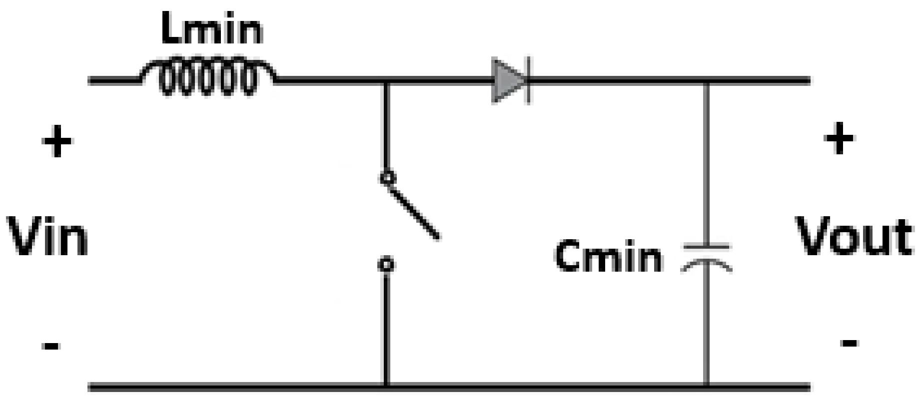

Source: The authors, 2026.

For the design of the converter, the following equations were used:

$$D = 1 - V_{in} / V_{out} \quad (1)$$

$$L_{min} = (V_{in} \cdot D) / (f_{sw} \cdot \Delta I_L) \quad (2)$$

$$C_{min} = (D \cdot P_{out}) / (f_{sw} \cdot \Delta V_{out} \cdot V_{out}) \quad (3)$$

Where:

D is the duty cycle (dimensionless);
L_{min} is the minimum inductance (H);
V_{in} is the input voltage (V);
V_{out} is the output voltage (V);
C_{min} is the minimum capacitance (F);
P_{out} is the output power (W);
f_{sw} is the switching frequency (Hz).

To ensure stability and proper tracking, the inductor was sized to guarantee that the converter operates strictly in Continuous Conduction Mode (CCM), which defines the acceptable inductor current ripple. Similarly, the capacitor was sized to ensure a maximum output voltage ripple of 1%, providing a stable DC-link voltage for the inverter stage. Based on these design criteria, the actual parameters implemented in the Simulink model consist of a switching frequency of 5 kHz, an inductance of 1.5 mH, and a capacitance of 1 mF.

2.4. Fault modelling

To evaluate the behavior of the photovoltaic generator under contingency conditions, the configuration shown in Figure 3 was adopted. The arrangement consists of a photovoltaic system, a DC–DC boost converter controlled by an MPPT algorithm, a three-phase DC–AC inverter, and the low-voltage grid represented by a balanced source of 120 V (rms), 60 Hz.

Figure 3 – Grid-connected photovoltaic system used in the simulations.

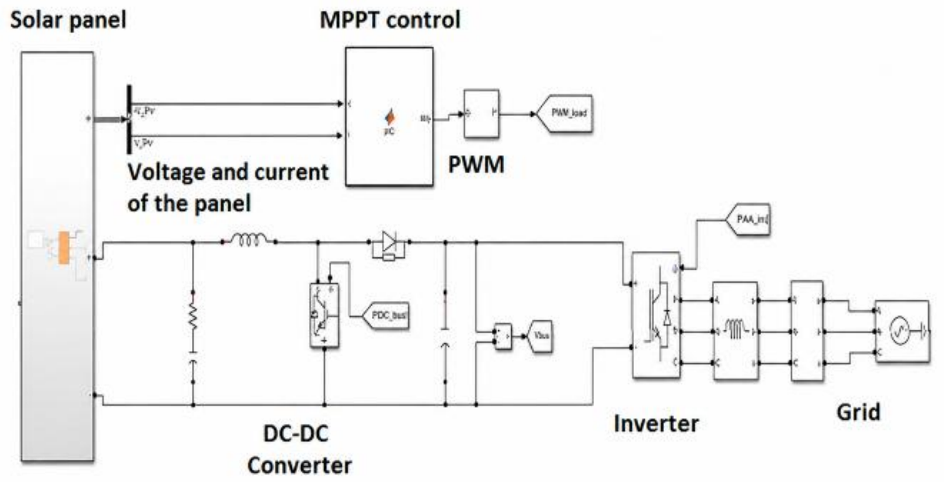

Source: The authors, 2026.

The selected fault scenarios are divided into DC-side and AC-side (grid-side) disturbances. DC-side faults (open-circuit, short-circuit, and partial shading) were chosen because they represent the most common internal failures caused by cable degradation, physical damage, and environmental changes respectively, directly impacting the MPPT efficiency (ALAM et al., 2015). The AC-side single-phase-to-ground fault was selected as it is one of the most frequent asymmetrical contingency in distribution networks, allowing the assessment of voltage sags and their propagation to the DC-link (KIM et al., 2009).

In all simulated scenarios, the fault is triggered at t = 0.35 s. This specific timeframe was adopted to ensure that the system's initial transients have completely decayed, the DC-link voltage has stabilized, and the MPPT algorithm has reached steady-state optimal convergence, thus providing a clear baseline for pre- and post-fault comparisons.

2.4.1. DC-side open-circuit fault

An open-circuit fault represents a break in the wiring connecting the panels. A switch was used to model this case, with the fault occurring at t = 0.35 s, triggered by a step block. The corresponding model is shown in Figure 4.

Figure 4 – Open-circuit fault in the photovoltaic array.

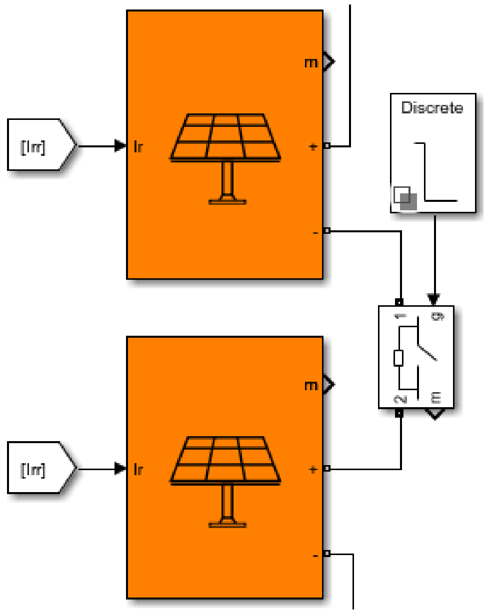

Source: The authors, 2026.

2.4.2. DC-side short-circuit fault

The same switch and step block were used to model the short-circuit fault, but in this case the switch is connected in parallel with the conductors submitted to the fault, as shown in Figure 5.

Figure 5 – Short-circuit fault in the photovoltaic array.

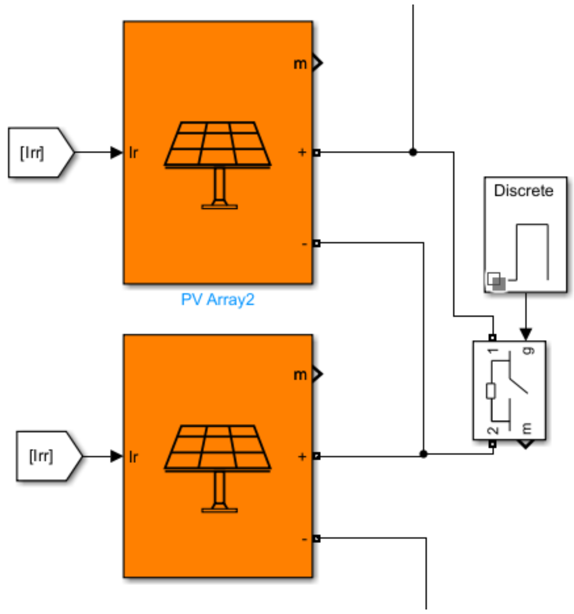

Source: The authors, 2026.

2.4.3. DC-side partial shading

This type of fault occurs when some solar panels in the array are subjected to a different irradiance level than the others. A step block was used, with initial irradiance of 1000 W/m² that suddenly drops to 500 W/m² at t = 0.35 s for one-third of the modules. The remaining panels continue at a fixed irradiance of 1000 W/m², as shown in Figure 6.

Figure 6 – Partial shading applied to one-third of the photovoltaic modules.

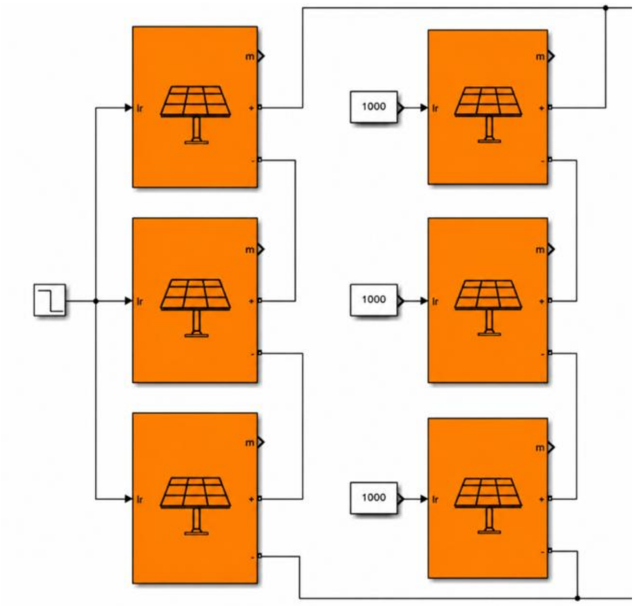

Source: The authors, 2026.

2.4.4. AC-grid-side fault

For the simulation of the fault at the grid side, a Three-Phase Fault block (capable of simulating three-phase faults, phase-to-phase faults and phase-to-ground faults) was connected between the inverter and the electrical grid. The configuration used corresponds to a single-phase-to-ground fault starting at t = 0.35 s and cleared at t = 0.40 s, as shown in Figure 7.

Figure 7 – Single-phase-to-ground fault at the grid side.

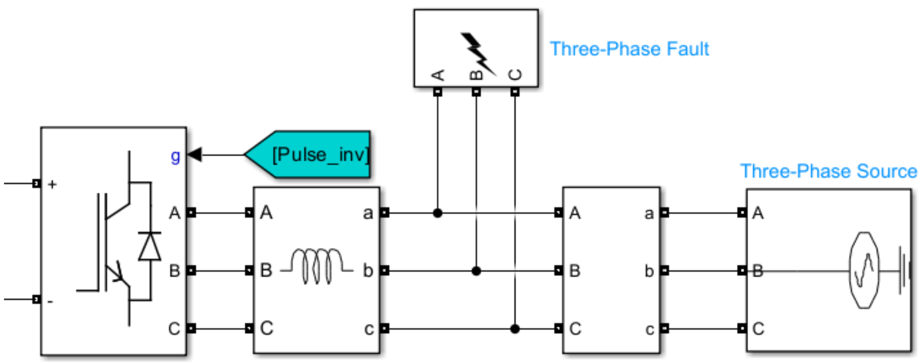

Source: The authors, 2026.

III. RESULTS

3.1. Normal operation

Under standard test conditions (1000 W/m², 25 °C) without faults, the system establishes a steady-state baseline to serve as a reference for analysis. The successful operation of the entire conversion process is first evidenced by the inverter's output, which injects balanced, 120°-phase-shifted sinusoidal AC currents into the 60 Hz grid, as illustrated in Figure 8. This grid integration confirms the accurate tuning of the inverter's current control loop.

Figure 8 – Three-phase currents injected into the grid under normal operation.

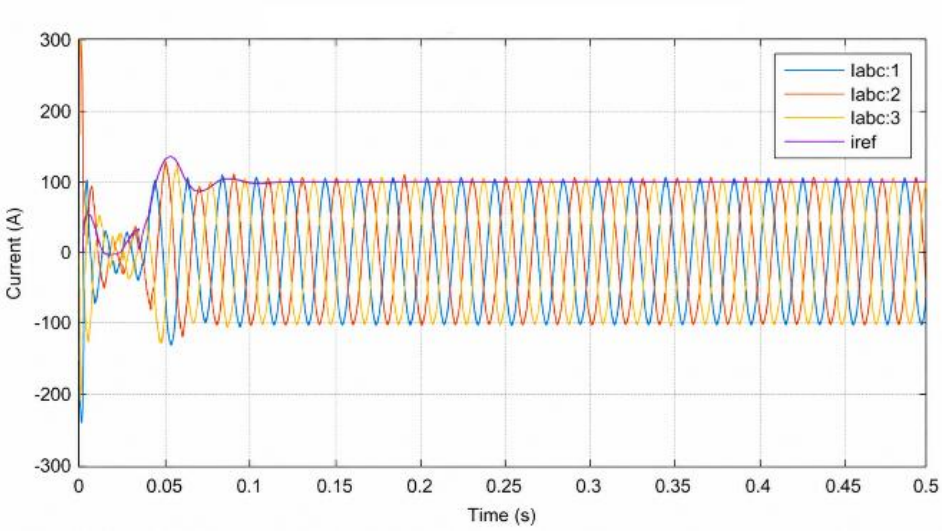

Source: The authors, 2026.

Figure 9 – DC-link voltage under normal operation.

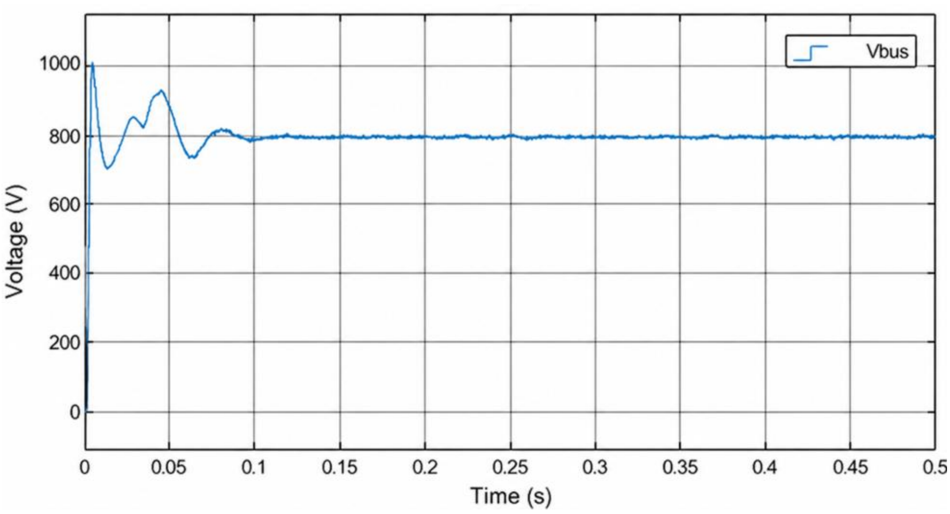

Source: The authors, 2026.

Figure 10 – Power generated by the photovoltaic array under normal operation.

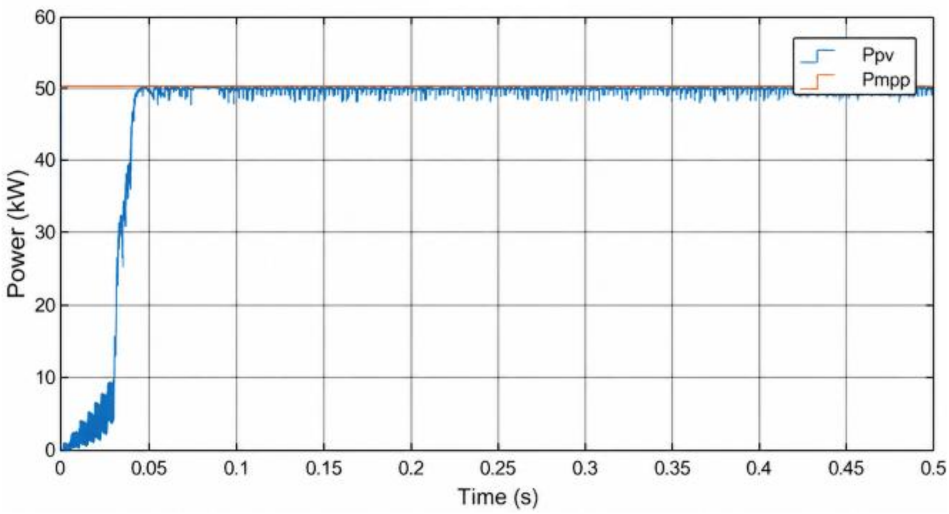

Source: The authors, 2026.

This stable AC output relies directly on the intermediate conversion stage, where the DC-link capacitor is regulated at its 800 V reference after a brief startup transient, as presented in Figure 9. The regulation of the DC-link voltage provides an operational condition for the inversion stage. Finally, maintaining this energy balance is ensured by the P&O MPPT algorithm, which successfully drives the boost converter to extract approximately 50 kW from the PV array, as shown in Figure 10. This extracted active power closely matches the theoretical maximum of 50.73 kW for the 238-module array. The minor steady-state power oscillations observed are an inherent and expected characteristic of the P&O algorithm continuously perturbing the operating voltage around the global maximum.

3.2. DC-side open-circuit fault

An open-circuit fault physically isolates one-third of the PV array at t = 0.35 s. This abrupt disconnection causes an instantaneous drop in the available DC current. To maintain the active power balance, the inverter controller rapidly reduces the amplitude of the injected AC currents, as reported in Figure 11, without losing grid synchronization or introducing significant harmonic distortion.

Figure 11 – Three-phase currents under open-circuit fault in the array.

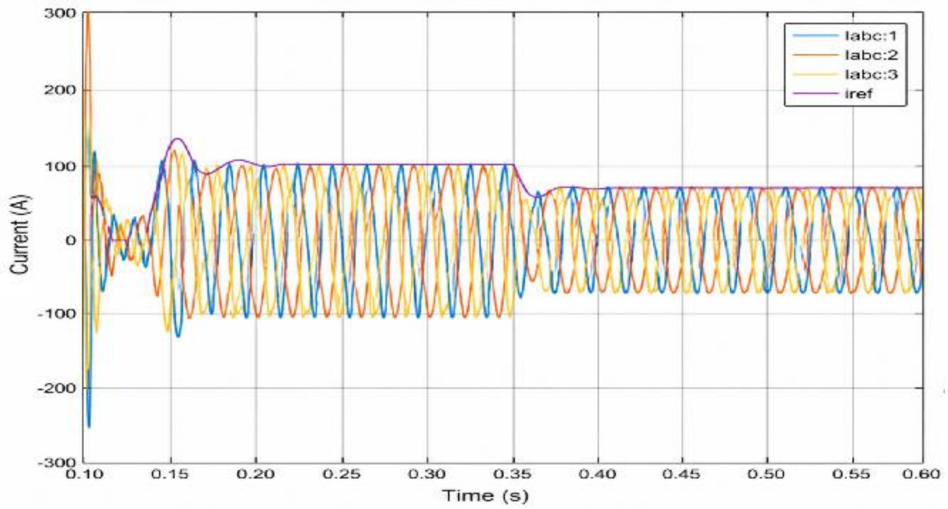

Source: The authors, 2026.

During this initial adjustment, because the inverter attempts to keep injecting the pre-fault power level for a fraction of a second, a temporary power mismatch occurs. This mismatch drains the DC-link capacitor, leading to a transient voltage dip, as evidenced by Figure 12. Despite the severe disturbance, the voltage control loop reacts, restoring the DC-link to the 800 V nominal level within a recovery time of approximately 0.1 s. Simultaneously, the MPPT algorithm converges to the new global maximum of the remaining active modules, stabilizing the extracted power at approximately 33.3 kW, as can be seen in Figure 13, which corresponds exactly to two-thirds of the array's nominal capacity.

Figure 12 – DC-link voltage under open-circuit fault.

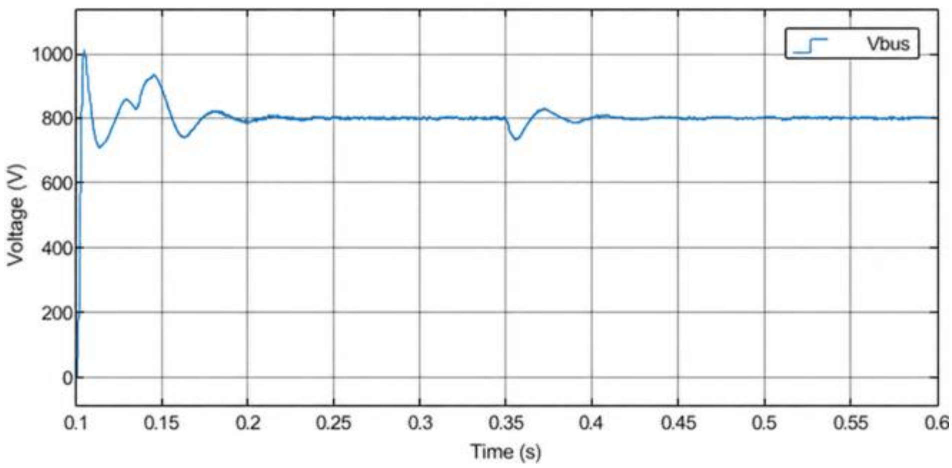

Source: The authors, 2026.

Figure 13 – Power generated by the photovoltaic array under open-circuit fault.

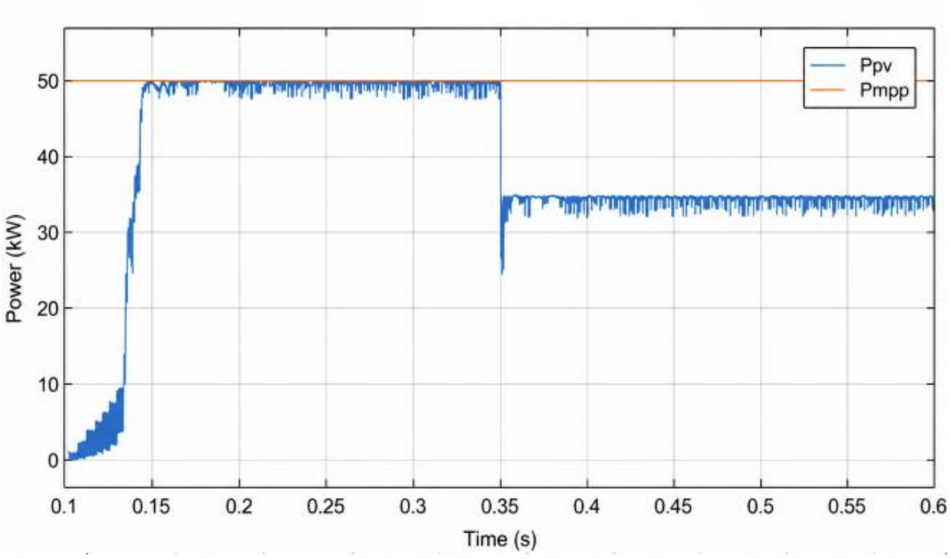

Source: The authors, 2026.

3.3. DC-side short-circuit fault

A short-circuit across one of the parallel strings at t = 0.35 s forces its terminal voltage to zero, representing a more severe dynamic challenge than an open-circuit. The sudden loss of generation capacity forces the grid-tied inverter to abruptly adjust the injected three-phase AC currents, as observed in Figure 14. The current controller successfully prevents instability, restoring a balanced, reduced-amplitude AC output within a few grid cycles, after 0.075 s.

Figure 14 – Three-phase currents under short-circuit fault in the array.

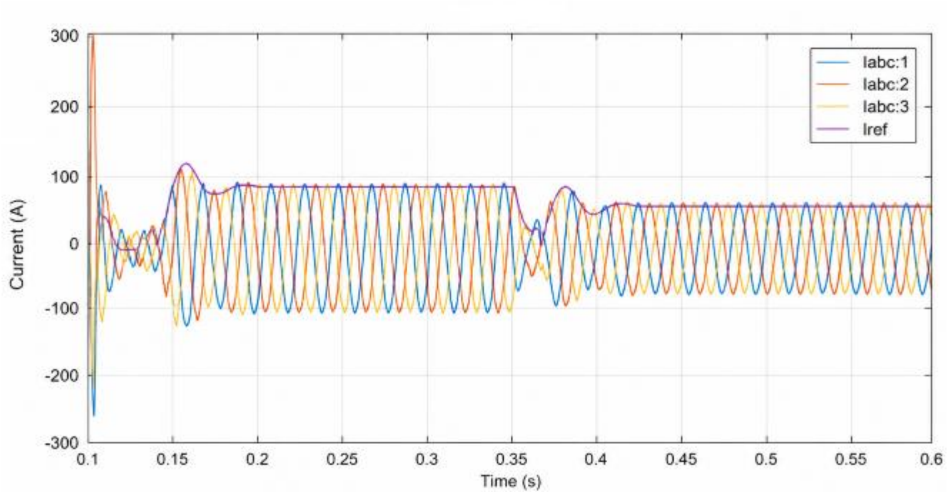

Source: The authors, 2026.

Internally, this fault creates an energy deficit. The DC-link voltage experiences a deep transient sag and exhibits larger oscillations, as shown in Figure 15, as the boost converter struggles to compensate for the collapsed string voltage. During the initial milliseconds of the fault, the transient mismatch is so extreme that the active power flow temporarily reverses, as illustrated in Figure 16. This negative power indicates that the DC-link capacitor temporarily absorbs energy from the AC grid to maintain the voltage level before the control loop saturates. Although the MPPT controller eventually recovers and stabilizes the extracted power at approximately 33 kW, this brief reverse power flow highlights a critical operational vulnerability that could trigger reverse-current protection relays or damage semiconductor switches if not properly mitigated.

Figure 15 – DC-link voltage under short-circuit fault.

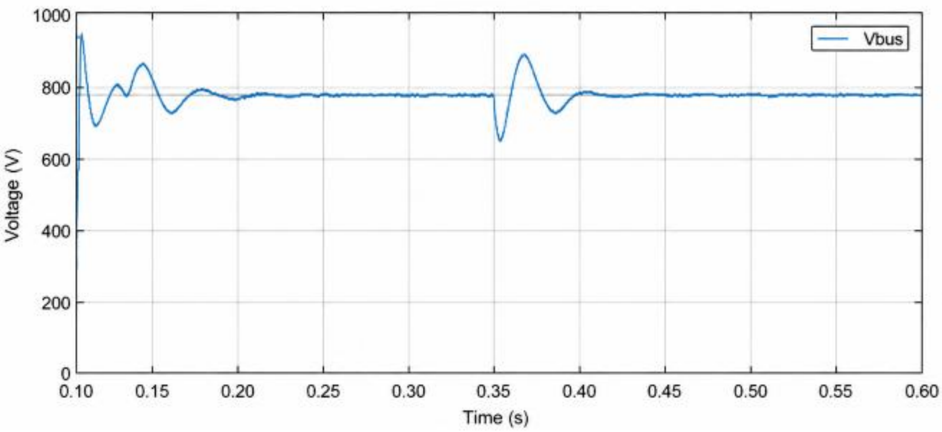

Source: The authors, 2026.

Figure 16 – Power generated by the photovoltaic array under short-circuit fault.

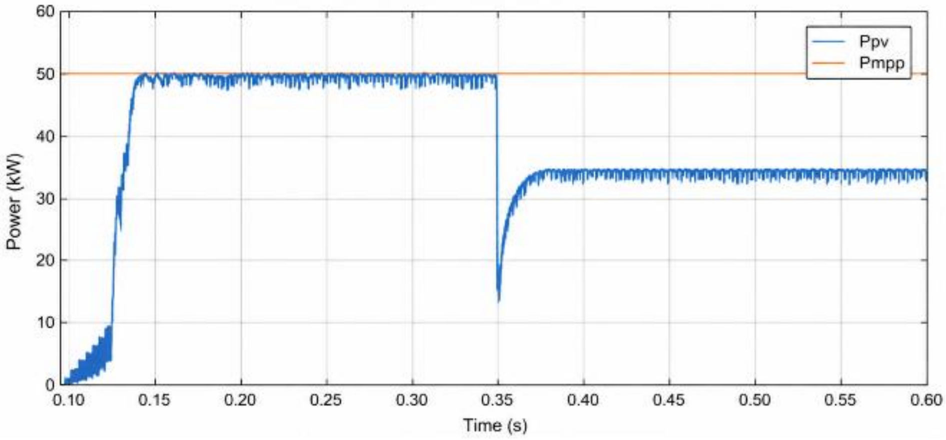

Source: The authors, 2026.

3.4. DC-side partial shading

In contrast to hard electrical faults, environmental disturbances such as partial shading impose a softer transient on the system. At t = 0.35 s, the irradiance on one-third of the modules is abruptly halved from 1000 W/m² to 500 W/m², simulating a fast-moving cloud. The inverter smoothly scales down the amplitude of the injected AC currents, as evidenced by Figure 17, to match the new energy equilibrium, preserving the sinusoidal waveform and the 120° phase shift without noticeable distortion.

Figure 17 – Three-phase currents under partial shading.

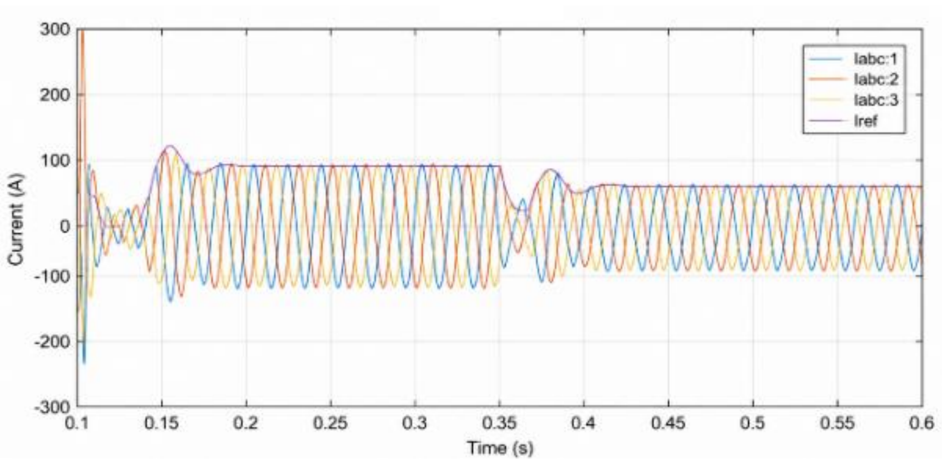

Source: The authors, 2026.

Because the affected modules continue to generate power at a reduced rate rather than being completely bypassed, the energy mismatch is minimal. Consequently, the DC-link capacitor experiences only a slight voltage dip, as can be seen in Figure 18, which is damped by the boost converter significantly faster than in the previous fault scenarios. The P&O algorithm successfully tracks the new maximum power point without being trapped in local minima, stabilizing the total generated power at approximately 41.6 kW, as presented in Figure 19. This represents a reduction of exactly one-sixth of the nominal capacity, confirming the control system's robustness to sudden meteorological variations.

Figure 18 – DC-link voltage under partial shading.

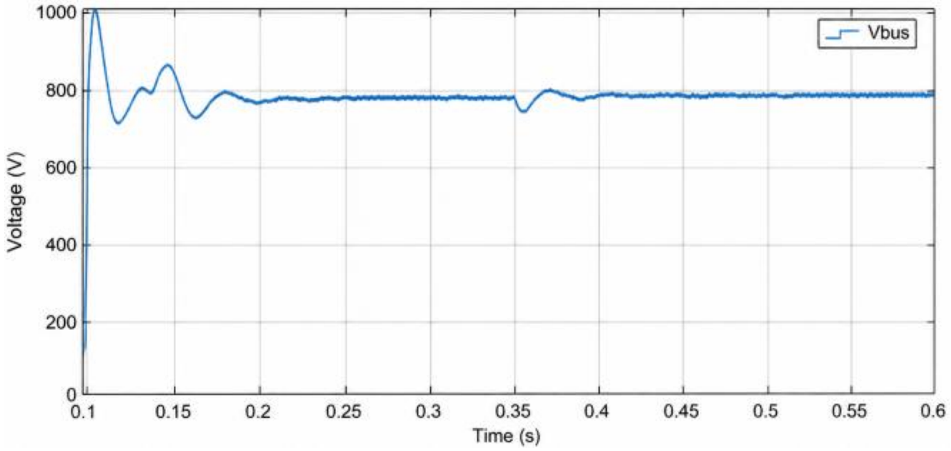

Source: The authors, 2026.

Figure 19 – Power generated by the photovoltaic array under partial shading.

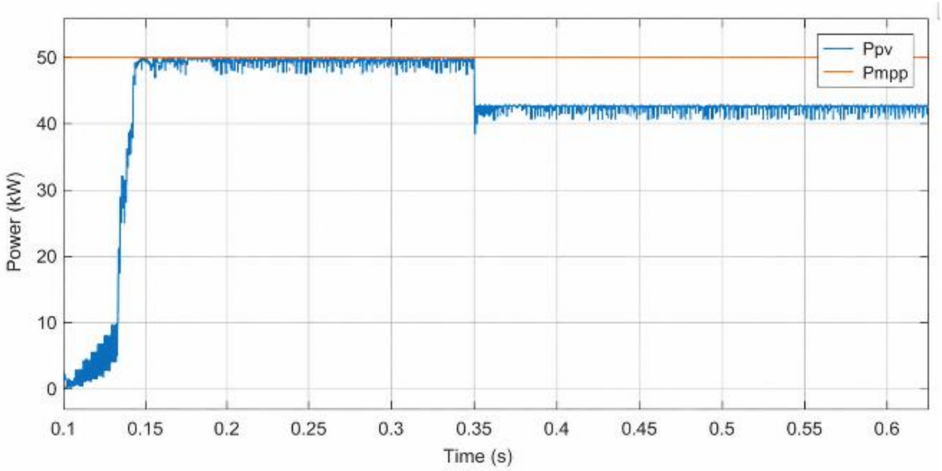

Source: The authors, 2026.

3.5. AC-side single-phase-to-ground fault

The external grid-side fault, applied to Phase C between t = 0.35 s and t = 0.40 s, imposes the most critical electrical stress on the entire conversion chain. The asymmetrical voltage sag severely disrupts the inverter's synchronization and control loops, resulting in highly distorted and unbalanced AC currents injected into the grid during the 50 ms fault window, as depicted in Figure 20.

Figure 20 – Three-phase currents under grid-side single-phase-to-ground fault.

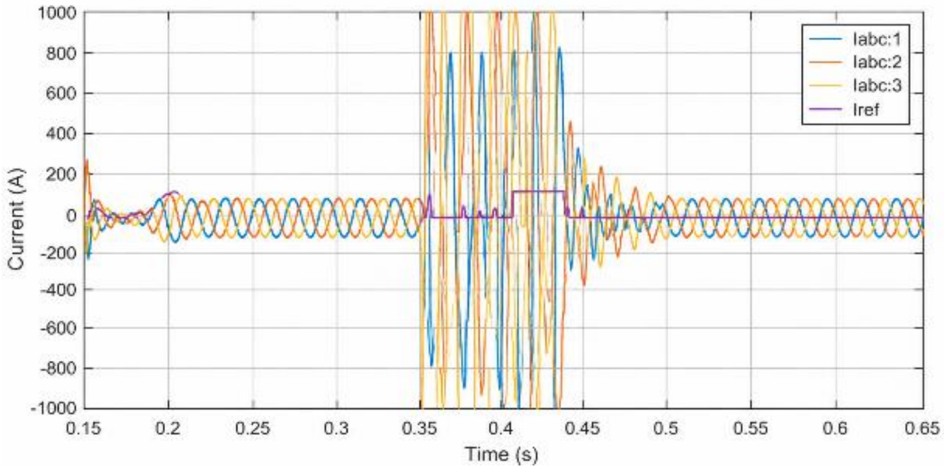

Source: The authors, 2026.

The physical consequence of the grid voltage collapse is a drastic reduction in the inverter's ability to export active power. However, the PV array and boost converter initially continue to pump maximum DC power into the system. This massive energy bottleneck forces the excess energy to accumulate in the DC-link capacitor, causing the DC voltage to increase to a peak of approximately 4000 V, as reported in Figure 21. This extreme overvoltage — five times the 800 V nominal rating — poses a severe threat to the dielectric integrity of the capacitors and the blocking voltage limits of the IGBTs. Consequently, the active power extracted from the PV array collapses almost entirely during the fault, as evidenced by Figure 22. Although the system recovers its nominal 800 V DC-link and pre-fault power levels approximately 0.15 s after the fault is cleared, these results quantitatively demonstrate the absolute necessity of implementing DC chopper circuits (braking resistors) and advanced Fault Ride-Through (FRT) control strategies to dissipate excess energy and protect the hardware during severe grid contingencies.

Figure 21 – DC-link voltage under grid-side single-phase-to-ground fault.

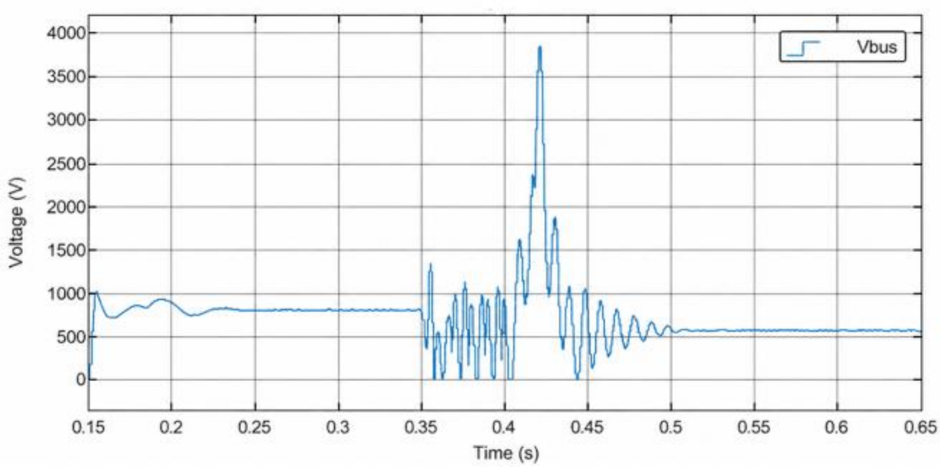

Source: The authors, 2026.

Figure 22 – Power generated by the photovoltaic array under grid-side single-phase-to-ground fault.

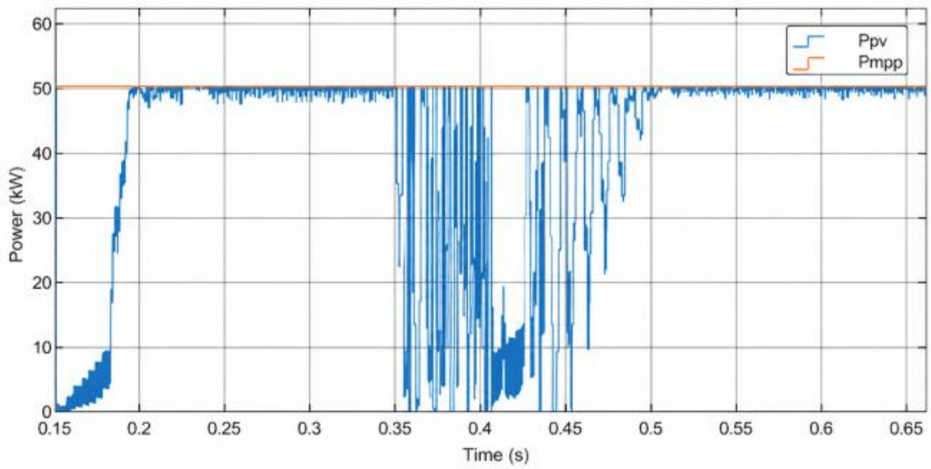

Source: The authors, 2026.

3.6. Discussion

The simulation results reveal distinct behavioral patterns depending on the origin of the fault, carrying practical implications for the design of PV protection schemes. For DC-side disturbances, such as open-circuits and partial shading, the system demonstrated inherent resilience. The P&O MPPT algorithm successfully converged to new stable operating points in less than 0.1 s. However, the DC short-circuit scenario introduced a transient reverse power flow. From a practical standpoint, this reverse current highlights the necessity of installing blocking diodes and fast-acting DC string fuses to prevent healthy modules from feeding power into the faulted string, thereby avoiding thermal damage and fire hazards.

Conversely, the AC-side single-phase-to-ground fault exposed the most severe vulnerabilities of the conversion chain. As documented in previous grid-integration literature (KIM et al., 2009), asymmetrical voltage sags severely limit the inverter's active power export capability. The simulated 4000 V DC-link spike illustrates the massive energy bottleneck that occurs when the PV array continues to generate maximum power while the grid cannot absorb it. Comparing these findings with standard industry practices (ALAM et al., 2015), this overvoltage dictates that commercial PV inverters must be equipped with DC chopper circuits (braking resistors) and Fault Ride-Through (FRT) control strategies to dissipate excess energy and protect the DC-link capacitors and IGBTs from dielectric breakdown.

Despite providing insights into transient electrical stresses, the developed model has certain limitations. First, the standard P&O MPPT algorithm, while widely used for its simplicity, is susceptible to steady-state oscillations and may trap the system in local power maxima under highly complex shading patterns, unlike more advanced heuristic methods. Second, the thermal dynamics of the PV modules were not considered; real-world faults would induce rapid temperature rises that further degrade efficiency and alter the current-voltage curves. Finally, the electrical grid was modelled as an ideal infinite bus, neglecting the impact of grid impedance and the PV system's potential contribution to local voltage regulation during the fault.

IV. CONCLUSION

This paper presented a comprehensive analysis of the electromagnetic transients and electrical stresses imposed on a 50.7 kW grid-connected PV system under various contingency scenarios. The main technical contribution lies in demonstrating that while standard control loops can effectively manage DC-side disturbances with rapid recovery times, severe AC-side faults expose the conversion chain to potentially catastrophic stresses, notably a DC-link overvoltage reaching 4000 V and transient reverse power flows.

These findings underscore the critical need for coordinated protection schemes, including DC blocking diodes and active Fault Ride-Through (FRT) mechanisms coupled with DC choppers, to ensure hardware integrity and grid stability. The current study is limited by the assumption of an ideal electrical grid and the absence of thermal dynamic modeling. Future research will focus on addressing these limitations by integrating advanced adaptive MPPT algorithms and implementing active FRT control strategies.

V. REFERENCES

ABDELSALAM, A. K. et al. High-performance adaptive perturb and observe MPPT technique for photovoltaic-based microgrids. ***IEEE Transactions on Power Electronics***, v. 26, n. 4, p. 1010-1021, April. 2011.

AGÊNCIA NACIONAL DE ENERGIA ELÉTRICA – ANEEL. **Resolução Normativa nº 482, de 17 de abril de 2012**. Diário Oficial da União, Brasília, DF, 19 Apr. 2012. Disponível em: https://www.gov.br/aneel/pt-br. Acesso em: 6 out. 2023.

AGÊNCIA NACIONAL DE ENERGIA ELÉTRICA – ANEEL. **SIGA – Sistema de Informações de Geração da ANEEL**: dados abertos. 2024. Available in: https://dadosabertos.aneel.gov.br/dataset/siga-sistema-de-informacoes-de-geracao-da-aneel. Accessed: 10 Mar. 2024.

ALAM, M. K. et al. A comprehensive review of catastrophic faults in PV arrays: types, detection, and mitigation techniques. ***IEEE Journal of Photovoltaics***, v. 5, n. 3, p. 982-997, May 2015.

ALDWANE, B. Modeling, simulation and parameters estimation for photovoltaic module. In: INTERNATIONAL CONFERENCE ON GREEN ENERGY, 2014, Sfax. **Proceedings** [...]. Sfax: IEEE, 2014. p. 1-6.

CELIK, A. N.; ACIKGOZ, N. Modelling and experimental verification of the operating current of mono-crystalline photovoltaic modules using four- and five-parameter models. ***Applied Energy***, v. 84, n. 1, p. 1-15, jan. 2007.

FARANDA, R.; LEVA, S. Energy comparison of MPPT techniques for PV systems. ***Journal of Electromagnetic Analysis and Applications***, v. 3, n. 6, p. 452-458, 2008.

GIRGIS, M. E.; ELKHATEEB, N. A. Enhancing photovoltaic MPPT with P&O algorithm performance based on adaptive PID control using exponential forgetting recursive least squares method. ***Renewable Energy***, v. 237, p. 121801, 2024.

GRAU, T.; HUO, M.; NEUHOFF, K. Survey of photovoltaic industry and policy in Germany and China. ***Energy Policy***, v. 51, p. 20-37, 2012.

KADEVAL, H. N.; PATEL, V. K. Mathematical modelling for solar cell, panel and array for photovoltaic system. ***Journal of Applied and Natural Science***, v. 13, n. 3, p. 937-943, 2021.

KIM, S.-K. et al. Modeling and simulation of a grid-connected PV generation system for electromagnetic transient analysis. ***Solar Energy***, v. 83, n. 5, p. 664-678, 2009.

KRISHNARAM, K. et al. Experimental design and analysis of advanced three phase converter for PV application with WCO-P&O MPPT controller. ***Scientific Reports***, v. 14, n. 1, p. 10984, 2024.

NKAMBULE, M.; HASAN, A.; ALI, A. MPPT under partial shading conditions based on perturb & observe and incremental conductance. In: INTERNATIONAL CONFERENCE ON ELECTRICAL AND ELECTRONICS ENGINEERING (ELECO), 11., 2019, Bursa. **Proceedings** [...]. Bursa: IEEE, 2019. p. 85-90.

SUSKIS, P.; GALKIN, I. Enhanced photovoltaic panel model for MATLAB/Simulink environment considering solar cell junction capacitance. In: ANNUAL CONFERENCE OF THE IEEE INDUSTRIAL ELECTRONICS SOCIETY (IECON), 39., 2013, Vienna. **Proceedings** [...]. Vienna: IEEE, 2013. p. 1613-1618.

TSAI, H.-L.; TU, C.-S.; SU, Y.-J. Development of generalized photovoltaic model using MATLAB/Simulink. In: WORLD CONGRESS ON ENGINEERING AND COMPUTER SCIENCE (WCECS), 2008, San Francisco. **Proceedings** [...]. San Francisco: IAENG, 2008. p. 1-6.

YAO, M.; CAI, X. An overview of the photovoltaic industry status and perspective in China. ***IEEE Access***, v. 7, p. 181051-181060, 2019.

ZAID, S. et al. Model-free predictive current control of a 3-φ grid-connected neutral-point-clamped transformerless inverter. ***Energies***, v. 16, n. 7, p. 3141, 2023.

VI. ACKNOWLEDGEMENTS

The authors would like to thank the Department of Electrical Engineering of the Federal University of Bahia (UFBA) for the technical and institutional support provided during the development of this research.

VII. COPYRIGHT